



# Facile low-temperature synthesis of nickel oxide by an internal combustion reaction for applications in electrochromic devices

Christian Lupo<sup>1</sup>, Florian Eberheim<sup>1</sup>, and Derck Schlettwein<sup>1,\*</sup> 

<sup>1</sup>Institute of Applied Physics and Center of Materials Research (ZfM), Justus-Liebig-University Giessen, Heinrich-Buff-Ring 16, 35392 Giessen, Germany

**Received:** 17 October 2019

**Accepted:** 18 June 2020

**Published online:**

13 July 2020

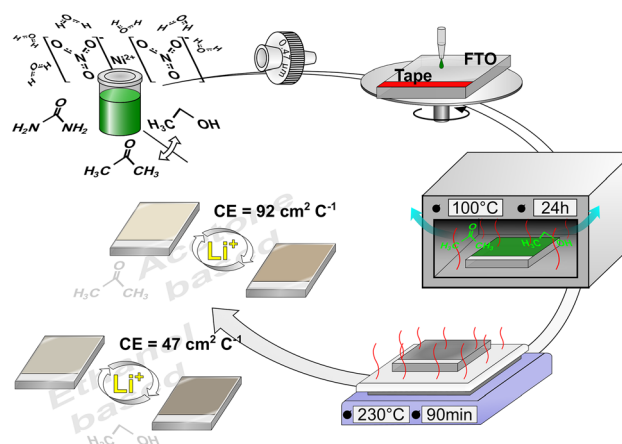
© The Author(s) 2020

## ABSTRACT

Electrochromic nickel oxide ion storage anodes compatible to tungsten oxide as cathode layer are prepared by a combustion reaction with urea as fuel and nickel nitrate as oxidizer at temperatures not higher than 230 °C to stay well within the temperature range in which thermally sensitive intercalated tungsten oxide layers are still stable. The precursors for nickel oxide are well available materials and the preparation of the layers can be performed at low energy input by spin-coating onto the substrate and moderate heating on a hot-plate. Ethanol and acetone were used as solvents and reveal large differences in the resulting film morphologies, electric and electrochromic characteristics. Cyclic voltammetry measurements in contact to lithium perchlorate (LiClO<sub>4</sub>) in propylene carbonate show remarkable colouration efficiencies at 550 nm of 47 cm<sup>2</sup> C<sup>-1</sup> for NiO prepared from ethanol solution and 92 cm<sup>2</sup> C<sup>-1</sup> for NiO prepared from acetone solution, which are, to the best of our knowledge, among the highest reported values for Li<sup>+</sup>-intercalation into NiO prepared at moderate substrate temperature reported so far.

Address correspondence to E-mail: schlettwein@uni-giessen.de

## GRAPHIC ABSTRACT



## Introduction

Energy saving is one of the relevant strategies to ensure sustainable modern societies [1]. Housing as one important sector offers great opportunities [2, 3]. Combinations of low-energy houses with green power generation units are already able to produce more power than they use (energy-plus houses) [4]. One of the key factors of this concept is the proper management of incoming and emitted heat [5, 6]. Aside from appropriate thermal insulation of walls, roofs and windows, the control of incoming solar radiation is important [7]. While in winter, incoming heat is mainly beneficial, in summer the benefits of room lighting have to be balanced against overheating of rooms which in many cases might then require energy-consuming air-conditioning by refrigeration [4]. Smart windows represent an efficient way to control the incoming heat by solar radiation [8]. Electrochromic devices, in which the transmission of light can be tuned electrically can form a relevant part of smart windows. They can easily be integrated into central building control systems to optimize the energy management. Commercial systems are available that can control the transmission of visible light between 9 and 51% with a solar heat gain coefficient between 8 and 36% [9]. Despite the fact that electrochromic windows are still quite expensive, they can be found in commercial and public buildings as well as

in the form of rear-view mirrors in automobiles, sunglasses or windows in the Boeing 787 Dreamliner [10–15]. Typical electrochromic devices consist of a tungsten oxide (WO<sub>3</sub>) colouring cathode, and an anodic counterpart of vanadium titanium oxide (almost not colouring) or nickel oxide (colouring) with Li<sup>+</sup> as intercalating ions and an ion exchange layer in between, typically an organic liquid or polymer gel electrolyte [16–19]. Nickel oxide (NiO) has a great potential to improve the overall characteristics of the devices due to the brown colouration upon oxidation and excalation of Li<sup>+</sup>, which perfectly fits to the blue colouration of reduced WO<sub>3</sub> upon intercalation of Li<sup>+</sup> to get a gradual and deeper darkening in a stack with minor changes in colour [16, 20, 21]. NiO is a well-known material to serve as counterpart for tungsten oxide and, because of the large number of possible manufacturing processes and precursor materials for its preparation, NiO offers great potential to meet the necessary technical requirements. As an inorganic material, e.g. used in combination with a transparent inorganic solid electrolyte such as lithium phosphorous oxynitride (LiPON) in an all-solid-state device, it preserves the high mechanical and thermal stability which can be of particular advantage when used with large-area electrochromic windows [22, 23]. When prepared to an equal thickness, e.g., it can store an identical amount of Li<sup>+</sup> as WO<sub>3</sub> [16, 24–28]. To improve the Li<sup>+</sup>-capacity and/or the diffusion coefficient of Li<sup>+</sup> in NiO mixed oxides with rare earth metals can be used

at, however, reduced electrochromic effect [29, 30]. On the way to an all-solid-state device, a solid Li<sup>+</sup>-conductor should replace the liquid or polymeric component [31]. To prepare such stacks it is mandatory that the preparation methods of the individual layers have to be compatible with already deposited materials. Therefore, the preparation for NiO has to fit, e.g., to the well-established WO<sub>3</sub> and a transparent solid electrolyte like LiPON. Tungsten oxide loses its excellent electrochromic characteristics at about 250 °C due to a phase transition [32]. LiPON can be prepared at moderate temperatures via sputtering deposition but shows high instability against water [33–36].

Nickel oxide is well available, of rather low toxicity and can be prepared by a variety of methods like electrochemical deposition [37–39], chemical bath deposition [40–43], flame/aerosol-assisted chemical-vapour-deposition [44–46] or sputtering [47–49]. Low processing temperatures are attractive to protect underlying layers in a given stack and to widen the range of applicable substrates. To reach sufficient NiO layer quality, however, a high substrate temperature of 300 °C or above is often needed during preparation or subsequent annealing as seen in a comparison across different methods of preparing NiO films (see Table 1 and Table S1). Among low temperature techniques like sputtering, electrochemical deposition, deposition of pre-formed nanoparticles [50] or pulsed laser

deposition which can even be performed with the substrate at room temperature [37], acceptable coloration efficiency could only be reached by electrodeposition or by spin-coating of pre-formed nanoparticles [50]. Sol–gel processes offer great possibilities to produce thin layers at moderate temperature, too, but with increasing film thickness the preparation becomes less reliable [51, 52]. All methods offer different advantages and disadvantages and must be selected depending on the needs and conditions in a given device structure. Therefore, a selection from a large variety of methods is important. By use of solution combustion synthesis (SCS), moderate process temperatures for NiO thin films with several nanometer thickness have also been reported [53–55]. Such layers, however, do not show sufficient lithium capacity to serve as counterpart to tungsten oxide in a smart window. To provide a beneficial electrochromic effect and to store an adequate amount of charge, a thickness of several hundred nanometers is mandatory.

In this work, we present an economic way to prepare NiO films with such increased thickness prepared below 250 °C. Some approaches to such films do exist in the literature. Zhang and Li reported a method in which they used nickel nitrate and urea as oxidizer and fuel to prepare thin films of approximately 65 nm at a temperature around 225 °C [54]. In

**Table 1** Coloration efficiency CE at the given wavelength  $\lambda$

EC active electrode layer	Method of film preparation	CE cm <sup>2</sup> C <sup>-1</sup> ( $\lambda$ /nm)	QA <sup>-1</sup> mC cm <sup>-2</sup>	QV <sup>-1</sup> */C cm <sup>-3</sup>	Q <sub>max</sub> V <sup>-1</sup> C cm <sup>-3</sup>	d/nm	T <sub>max</sub> /°C	Ref
NiLiO	Spray deposition	33 (670)	np	np	np	np	np	[56]
NiO	Hydrothermal method	89 (550)	7.95 <sup>a</sup>	53	180 <sup>a</sup>	1500	400	[57]
NiO, LiNiO, NiO-PEG, LiNiO-PEG	Spray pyrolysis	41 (550)	16.6 <sup>b</sup>	698	np	240	350	[58]
Li–NiO	Sol–gel	34 (500)	2.4 <sup>a</sup>	240	690 <sup>a</sup>	100	300	[51]
NiO	Sputtering	38 (550)	8.49 <sup>a</sup>	283	np	300	~ 25	[47]
NiO	Spin-coating	115 (550)	1.34	89	np	150	150	[50]
LiNiO (gel-polymer not PC)	Sputtering	32 (550)	11.9	597	np	200	~ 25	[59]
NiO	Internal combustion (ethanol)	47 (550)	5.53	158	3260	350	230	tw
NiO	Internal combustion (acetone)	92 (550)	2.84	63	1020	450	230	tw

Corresponding charge per area  $Q/A$  and charge per volume  $Q/V$  as well as the achieved maximum volume charge density  $Q_{max}/V$  for LiClO<sub>4</sub>-PC based devices, film thickness  $d$  and highest temperature  $T_{max}$  applied during processing of nickel oxide on the substrate prepared by different techniques. For publications referring to more than one material, the sample with the highest CE value is listed. See Table S1 (Supplemental Information) for an extended comparison to OH<sup>-</sup> based devices

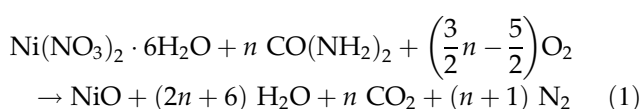
np not provided, tw this work

<sup>a,b</sup>Value not explicitly provided but extracted/calculated from <sup>a</sup>graphical data; <sup>b</sup>CE and  $\Delta OD$

\*Calculated from  $Q/A$  and  $d$

a series of experiments we did not manage to scale up this method towards several hundred nanometers of NiO.

Aside from the selection of fuel and oxidizer, the ratio of the two serves to optimize the combustion synthesis. By varying this ratio the reaction can be directed to different products, as shown by Bai et al., where the combustion of nickel nitrate with acetyl acetone or glycine leads to metallic nickel or nickel oxide or a mixture of both [55]. According to González-Cortés and Imbert [60], the overall reaction in a combustion synthesis with nickel nitrate and  $n$  mole urea, with a fuel to oxidizer ratio corresponding to the ratio of total valences of  $3/5 n$ , can be written as:



In the present method, however, organic solvents were used instead of water, the precursor concentration was higher and thicker films were achieved than in typical SCSs [21, 61]. In addition, the combustion reaction is based on precipitated precursors in the form of dried films. Because of these substantial differences to SCS, we just use the term combustion synthesis (CS) for this method.

In the following, we present a facile method to prepare thin films of nickel oxide of several hundred nanometres thickness which can be used as anodic electrochromic layers. The components are readily available, no vacuum process is necessary and routine lab equipment suffices. The method yields sufficient film thickness at low preparation temperatures, which provides full compatibility to other components in electrochromic cells. We, therefore, believe that this new preparation method can contribute to develop efficient electrochromic windows that are well affordable, and that may lead to widespread commercialization and significant contributions to energy-saving in modern architecture.

## Experimental

For all experiments we approached the solubility limit of nickel nitrate. Therefore, 8.00 mg or 7.12 mg  $\text{Ni}(\text{NO}_3)_2 \cdot 6 \text{H}_2\text{O}$  (98%, Alfa Aesar) were completely dissolved in 5.1 ml ethanol ( $\geq 99.9\%$ , Roth) or 8.0 ml acetone ( $\geq 99.5\%$ , Roth), respectively, and were allowed to rest overnight, before 0.5508 g or

0.4902 mg urea ( $\geq 99.5\%$ , Sigma Aldrich) were added, respectively, to establish a molar ratio of 1/3 between the nickel and urea and were allowed to rest overnight, again. Finally, the solutions were filtered by a  $0.47 \mu\text{m}$  Teflon filter and were observed to be stable for months. As substrate, fluorine doped tin oxide glass (FTO) (Zhuhai Kaivo,  $< 15 \Omega \text{sq}^{-1}$ ) was used, which had been cut and cleaned by RBS® 35 solution containing sodium hydroxide, tetrapotassium diphosphate, sodium carbonate, sodium hypochlorite and surfactants (Roth), acetone (Roth,  $\geq 99.5\%$ ) and isopropanol (Roth,  $\geq 99.8\%$ ) in an ultrasonic bath for 15 min each. Directly before the spin-coating process the FTO substrates were UV-ozone-treated for 10 to 15 min. The NiO films were prepared by spin-coating with 4000 rpm for the ethanol (ethNiO) or 3500 rpm for the acetone (aceNiO) based solution for 30 s. The optimum rotation speed to reach a homogenous coverage and a uniform film thickness for the different solutions had been determined in separate experiments before. The samples were then dried at  $100^\circ\text{C}$  for at least 20 h in an oven and finally annealed at  $230^\circ\text{C}$  for 90 min on a heat plate. Figure 1 shows a schematic representation of the procedure.

Thermogravimetric analysis (TGA) and differential thermal analysis (DTA) were performed on a Setsys Evolution 16/18 system under argon atmosphere. Samples for the TGA/DTA analysis were prepared as the films on FTO, but directly in the ceramic crucible. The resulting masses of the intermediate products in the crucibles, which were initially completely filled with solution, after drying for 24 h, were 23.3 mg and

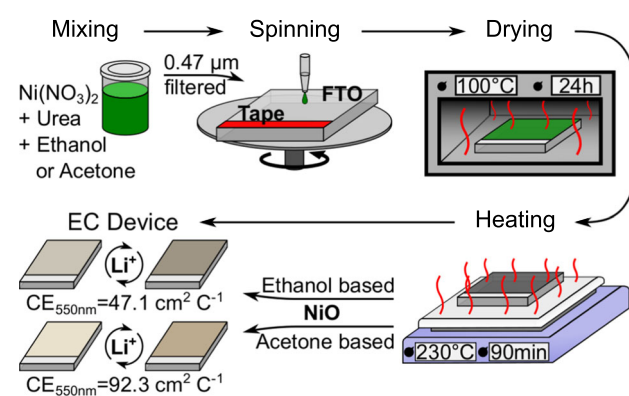


**Figure 1** Schematic representation of the facile combustion synthesis procedure of nickel oxide optimized for electrochromic applications. The colours of the EC devices represent the real optical impression measured by a spectrometer and calculated to RGB values by use of the D65 standard illumination (see S1).

15.6 mg for ethNiO and aceNiO, respectively. Samples were heated from room temperature to 230 °C at 24 K h<sup>-1</sup> and kept at this temperature for 2 h. X-ray diffraction (XRD) was performed on a Siemens D5000 using Cu K $\alpha$  for samples prepared as described for the TGA/DTA but in a ceramic vessel and from 10 ml of solution. Up to 20 h at 230 °C annealing were needed for a complete conversion from the green precursor to the black final product for the XRD analysis. High resolution scanning electron microscopy (SEM) was performed on a Zeiss MER-LIN with an acceleration voltage of 5 kV, an emission current of 120 pA and charge compensation with ionized N<sub>2</sub>. Cyclic voltammetry experiments were performed by use of an IviumStat (Ivium Technologies) with a scan rate of 50 mV s<sup>-1</sup> and vertex potentials of -1.2 V and 1.5 V vs Ag/AgCl, if not otherwise noted. Spectroelectrochemical characteristics were determined with the cell placed in a light-tight box by simultaneous use of an Evaluation Line (tec5) optical spectrometer with a spectral range of 310–1100 nm (specified range 360–900 nm). Reference spectra were obtained by use of the empty box. A three electrode setup was used with a platinum wire as counter electrode and a leak-free Ag/AgCl (242 mV vs SCE, Harvard Apparatus) as reference electrode. 1 mol L<sup>-1</sup> lithium perchlorate ( $\geq 95\%$ , Sigma-Aldrich) in propylene carbonate (anhydrous, Sigma-Aldrich) was used as an electrolyte.

The colouration efficiency CE was calculated by use of the wavelength dependent transmission  $T$  for the intercalated and the de-intercalated case (denoted by indices  $i$  and  $d$ ) and the observed charge density  $\Delta Q$ :

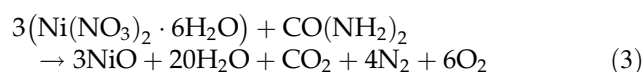
$$CE = \frac{\log_{10} \left[ \frac{T_i}{T_d} \right]}{\Delta Q} \quad (2)$$

Additionally, we use a calculated visual representation of the colour of films. The calculations were performed according to CIE (International Commission on Illumination) standards by use of an algorithm from the NVIDIA cooperation (more details in the Supplemental Information). In short, the transmission spectra of the sample, D65 illumination and the sensitivity of a typical human eye are used to calculate XYZ colour coordinates, which are converted to the corresponding RGB values. Superior to photographs, such calculated colours are independent of any camera and its position, any contrast and

brightness settings, background and ambient light, etc. Furthermore, they can directly be generated from spectra collected during spectroelectrochemical measurements which would not have been possible by use of a camera.

## Results and discussion

Films of NiO were prepared (Fig. 1) from mixed solutions of Ni(NO<sub>3</sub>)<sub>2</sub> and urea with ethanol (ethNiO) or acetone (aceNiO) as solvent. Other solvents were also tested but with ethanol and acetone the best film quality was obtained. Precursor films also formed from 1-propanol, but films peeled off from the substrate during the combustion reaction (CR). With dimethyl sulfoxide the whole material was spun off the substrate in the coating step. When using highly concentrated water-based solutions (essential to reach high films thickness), too much gaseous products were generated during the CR, leading to large bumps in the film. For ethanol and acetone, the spinning rate, drying time and temperature were varied in a wider range and the optimum conditions were chosen as indicated above. 230 °C was determined as the minimum temperature for ignition of the CR by observing a dried film on a hot plate which was slowly heated from room temperature under detailed monitoring of the surface temperature. With  $n = 1/3$  according to the ratio of reactants and according to (1), after rearrangement and multiplication by three, the reaction equation of the present combustion reaction reads:



Using the present ratio  $n = 1/3$  ambient oxygen is not needed for the combustion. The end of the conversion to NiO during the heating process can be observed by a change from the complete transparent state to a yellowish/brownish colour, which occurs after approximately 1.5 h. A delayed ignition of the CR is thereby indicated which can be caused by a chain breaking mechanism [62] as directly proven by the TGA analysis of a powder sample (Fig. 2).

In Fig. 2a the mass loss in percentage (line connected circles), the heat flow in  $\mu\text{V}$  (lines) for ethNiO (black) and aceNiO (red) and the applied temperature (green line) are plotted against the time. From 0 min (room temperature) up to 525 min (230 °C) a



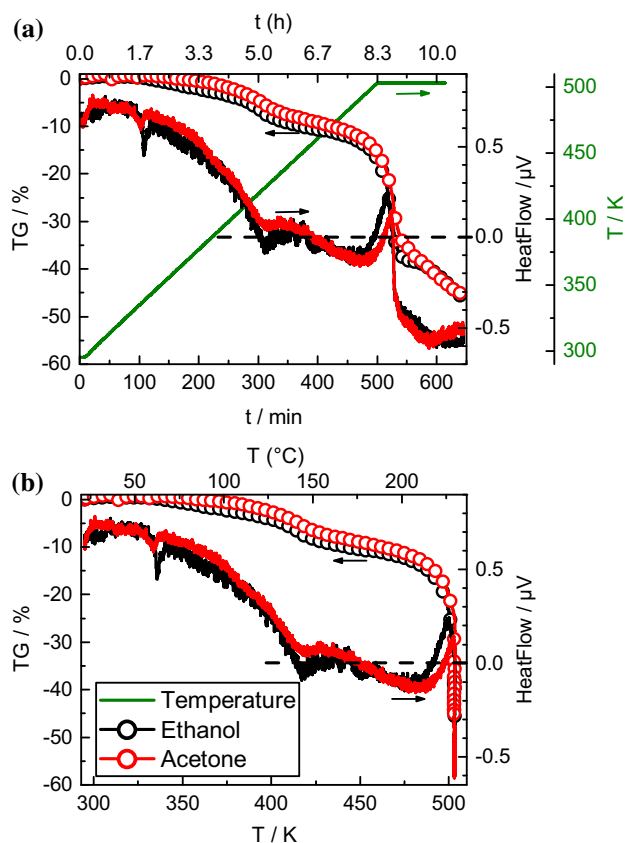


**Figure 2** Thermogravimetric (TG) and differential thermal (HeatFlow) analysis of the combustion synthesis of NiO from an ethanol based (black circles and lines) and an acetone based (red circles and lines) precursor. In **a** the percentaged mass change, the heat-flow and the temperature (green line) against the time is plotted. In **b** the graphical representation of TG and the HeatFlow values against the applied temperature are shown.

constant heating rate of  $24 \text{ K h}^{-1}$  was applied. In Fig. 2b the same data for ethNiO and aceNiO are shown with respect to the applied temperature. In the beginning of the analysis at approximately  $60^{\circ}\text{C}$  a little but ongoing loss in mass can be detected, which comes along with a sudden but short decrease in the heat flow for both ethNiO and aceNiO. This is surprising since the materials had been dried for at least 20 h at  $373 \text{ K}$  ( $100^{\circ}\text{C}$ ) before the TGA/DTA analysis. Melting of  $\text{Ni}(\text{NO}_3)_2 \cdot 6 \text{ H}_2\text{O}$  is known to occur around  $56^{\circ}\text{C}$  [63], indicating that some water had re-adsorbed before the TGA/DTA analysis leading to the re-formation of  $\text{Ni}(\text{NO}_3)_2 \cdot 6 \text{ H}_2\text{O}$  and gets released at around  $60^{\circ}\text{C}$  again.

The heat flow then decreases for both precursors up to ca.  $140^{\circ}\text{C}$ —the temperature where urea starts to decompose [63]—from where on it stays around

zero. In parallel, the rate of mass loss decreases. Chain breaking is thereby shown and obviously has reached a level, where as much heat is produced by the CR as consumed by further drying. While for ethNiO the heat flow crosses the zero line several times between  $140$  and  $175^{\circ}\text{C}$  the heat flow stays slightly positive for aceNiO throughout this regime. Beyond  $175^{\circ}\text{C}$  the heat flows get negative showing the exothermic character of the reactions still, however, without a significant increase in the rate of mass loss. Only at an applied temperature around  $210^{\circ}\text{C}$ , the rates of mass loss increase and around  $215^{\circ}\text{C}$  for ethNiO and  $225^{\circ}\text{C}$  for aceNiO the ignition is reached indicated by a rapid mass loss and significant changes in heat flow. Following an intermediate rise to the positive region presumably related to phase transitions into the gaseous products of Eq. (3) the heat flow shows a strongly exothermic reaction characteristic for the reaction enthalpy of (1). Consistently, this temperature had also turned out as the optimum reaction temperature of film formation (Fig. 1). The highly exothermic character of (1) is consistent with the reported temperatures up to  $973 \text{ K}$  ( $700^{\circ}\text{C}$ ) for the nickel nitrate urea combustion when performed under adiabatic conditions [60].

The XRD analysis in Fig. 3 clearly shows the complete conversion to NiO for both precursors. The ethNiO and the aceNiO diffraction pattern in black and red, respectively, perfectly fit to the cubic fcc structure measured for powder of NiO (ICSD 98-064-6098) depicted in green. Quite comparable relative peak intensities obtained for the films and the powder show the formation of crystalline films with random crystal orientation. Rather broad peaks are observed for the films and by applying the Scherrer equation to the peaks at approximately  $37^{\circ}$  we calculate an average crystal size of  $22.9 \text{ nm}$  for ethNiO and  $23.4 \text{ nm}$  for aceNiO, indicating crystals of quite similar size in the films prepared from both solvents.

The resulting film morphologies characterized by SEM are shown in Fig. 4. The cross-sections and the top views of the films show the high homogeneity of both NiO layers. They have a thickness of approximately  $350 \text{ nm}$  for the ethNiO and  $450 \text{ nm}$  for the aceNiO. This trend was also confirmed when the spin-coating was done with the same rotation speed despite higher precursor concentration in ethanol than acetone based solution. A closer look to (a) and (c) reveals, that the aceNiO layer seems to be more porous. Especially close to the FTO layer larger

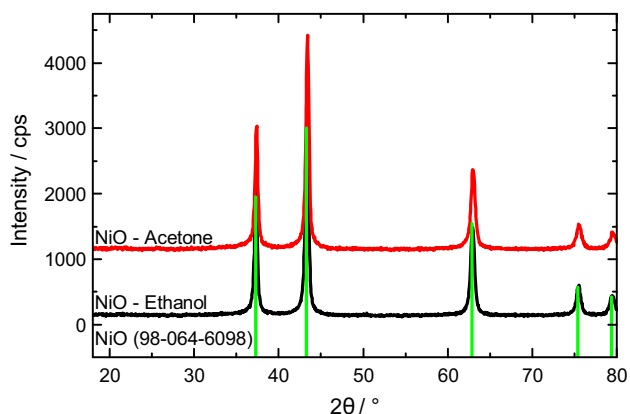


**Figure 3** XRD analysis of powder samples prepared by the combustion synthesis of nickel nitrate with urea and ethanol (black) and acetone (red) as solvent, respectively. In green the NiO reference from ICSD 98-064-6098 is shown.

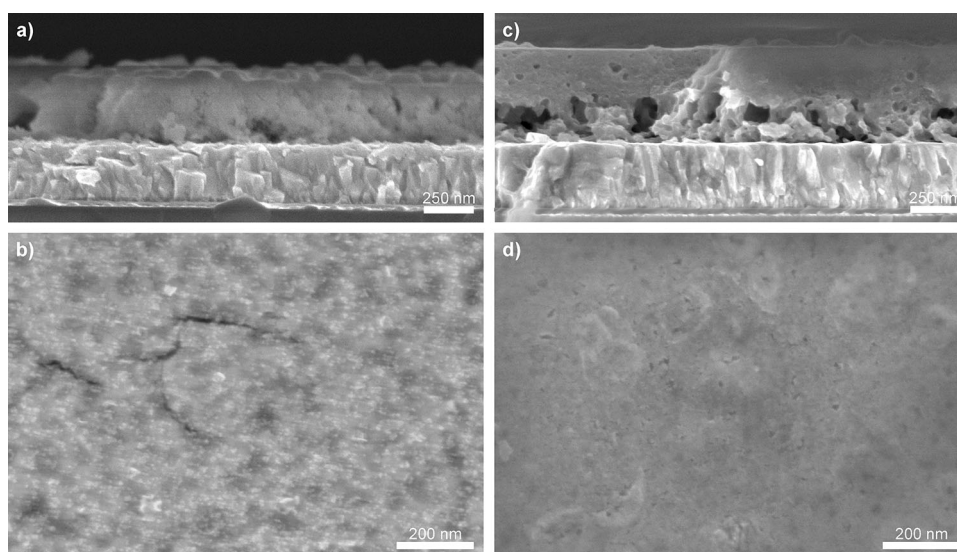
cavities can be found, which would explain the higher thickness for a given amount of material. Corresponding inhomogeneities can also be seen on top of the surface in (d). Small holes between 1 and 10 nm can be identified. The ethNiO layer, on the other hand, shows more grains but a widely closed structure aside from a few little cracks distributed over the layer.

The cyclic voltammograms for the first 10 cycles in Fig. 5 look qualitatively similar for ethNiO and aceNiO but show an almost doubled current density for the layer obtained from the ethanol-based precursor solution in contrast to the lower film thickness, indicating more efficient charging. For both samples, the initial cycle is consistently measured at slightly

different current density indicating a slight conditioning toward  $\text{Li}^+$ -intercalation. For subsequent cycles, however, a steady state is reached within about four cycles. Even the positions of the cathodic peaks at 0.0 V (I red) and 0.5 V (II red) and the anodic peak at 0.3 V (I ox) are quite fixed from the beginning. Just the second anodic peak (II ox) with 0.9 V for the aceNiO is a little bit shifted to a more positive value from 1.0 V for the ethNiO. The cycling behaviour of the spectroelectrochemical response of the ethNiO and aceNiO layers, also shown in Fig. 5, are in accordance to the observations of Granqvist et al. [48]. The transmittance of the initial state is found close to the average of the coloured and bleached states. Although the ethNiO is thinner than the aceNiO layer the overall transmittance of ethNiO is lower. Granqvist et al. showed that the transparency of NiO relates to a non-stoichiometric content of oxygen. They observed decreasing transparency for  $\text{NiO}_x$  layers with increasing  $x$ . It is thereby indicated that ethNiO is characterized by higher  $x$  in  $\text{NiO}_x$  than aceNiO.

A closer look to the peak current densities of I and II plotted in Fig. 6 reveals more differences. Compared to ethNiO, aceNiO shows much less variation in the peak current densities during cycling. Especially the second oxidation/reduction process (II) at aceNiO quickly establishes a steady state. Generally, a quite parallel increase of absolute current densities is observed for all peaks. The observed changes seem to refer to an identical underlying process. In the context of the results of Granqvist et al. [48] and

**Figure 4** Cross-section (a, c) and top-view (b, d) SEM images of the combustion-synthesised NiO films from an ethanol-based (a, b) and an acetone-based precursor solution (c, d).



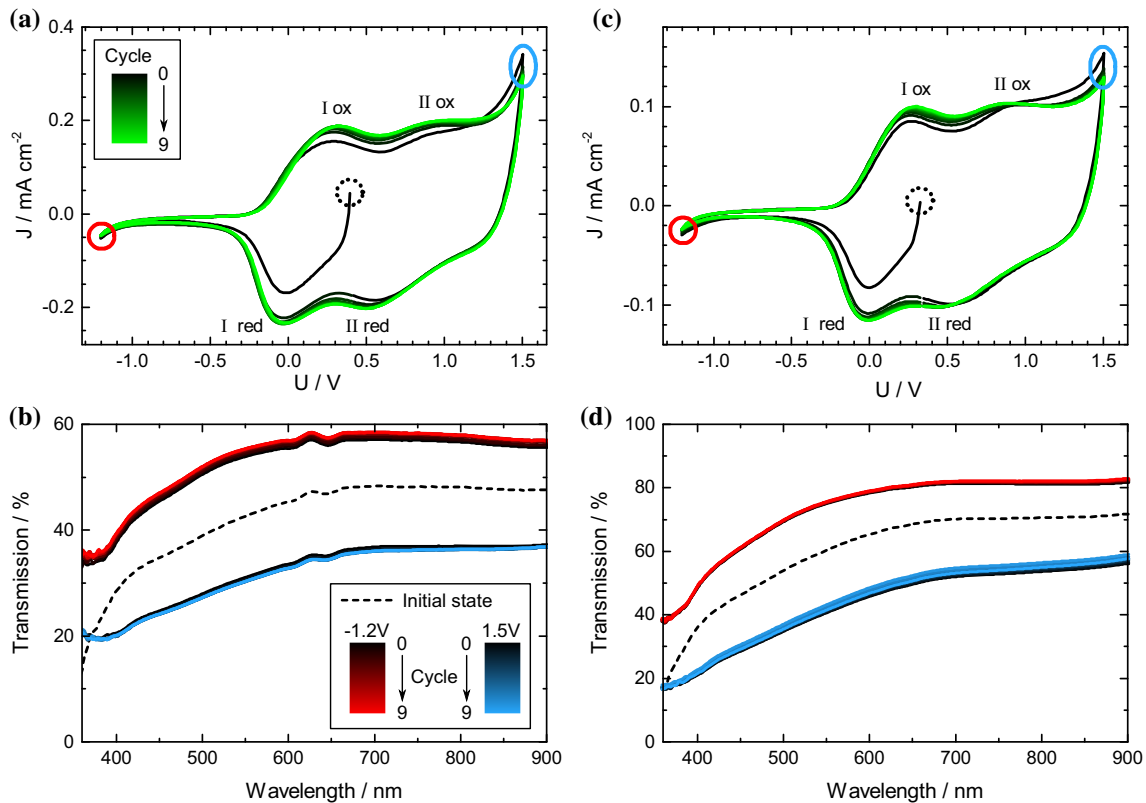


**Figure 5** Initial and subsequent nine cyclic voltammograms (a, c) and transmission spectra measured at the vertex potentials (b, d) of an ethNiO layer (a, b) and an aceNiO layer (c, d) starting

Rouquier et al. [64] this could indicate irreversible surface reactions of NiO with the anions and cations of the electrolyte upon cycling. In Fig. 7, the charge density for each cycle is plotted for the two kinds of films ethNiO and aceNiO. The initial cycle now appears significantly shifted from all subsequent cycles for both materials and a charge density unlike zero can be observed at the end of all cycles, in particular for the first cycles and for cycles of ethNiO whereby an ongoing modification might be indicated.

Clear electrochromic switching was observed for ethNiO and aceNiO. The ethNiO film changes its transparency at 550 nm by  $\Delta T = 25\%$  from 30.4 to 55.3% and the aceNiO sample by  $\Delta T = 34\%$  from 41.5 to 75.7% despite smaller charge exchanged by aceNiO compared with ethNiO (Fig. 5). A colouration efficiency of  $47.1 \text{ cm}^2 \text{ C}^{-1}$  at 550 nm is calculated for ethNiO and of  $92.3 \text{ cm}^2 \text{ C}^{-1}$  for aceNiO upon cycling between 1.5 V and -1.2 V which is one of the highest values for NiO in  $\text{LiClO}_4/\text{PC}$  reported (see Table 1). The scan rate of  $50 \text{ mV s}^{-1}$  results in a corresponding switching time of 54 s, considerably shorter than

with the black lines and proceeding to the coloured line with the initial transmission spectra shown as dashed line.

10 min which are typical for use in smart windows [65, 66]. To explore the maximum accessible switching range, potential steps of  $-2 \text{ V}$  and  $+2 \text{ V}$  were applied for 90 s (Fig. 8) each. ethNiO shows a change from 23.4 to 56.8% and the aceNiO sample a change from 26.5 to 81.1% in transmission at 550 nm. This corresponds to changes of  $\Delta T = 33\%$  and  $\Delta T = 55\%$  for the two materials, respectively, and can be considered technically attractive. Whereas, the derived parameters differ significantly from the cyclic voltammogram to the double potential step measurement, this is not the case for the colour impression, as can be seen by comparing the top and bottom part of Fig. 8. The colours surrounding the data points are calculated from the collected spectra (as described in the supplementary information) and represent the visual colour impression very well. The cycle in Fig. 8a shows a CE of  $92 \text{ cm}^2 \text{ C}^{-1}$  for the sweep from  $-1.2 \text{ V}$  to  $1.5 \text{ V}$  but the last potential step in Fig. 8b provides a CE of only  $20 \text{ cm}^2 \text{ C}^{-1}$ , without significant differences in the optical impression. The switching time of 2.3 s to reach 90% of maximum



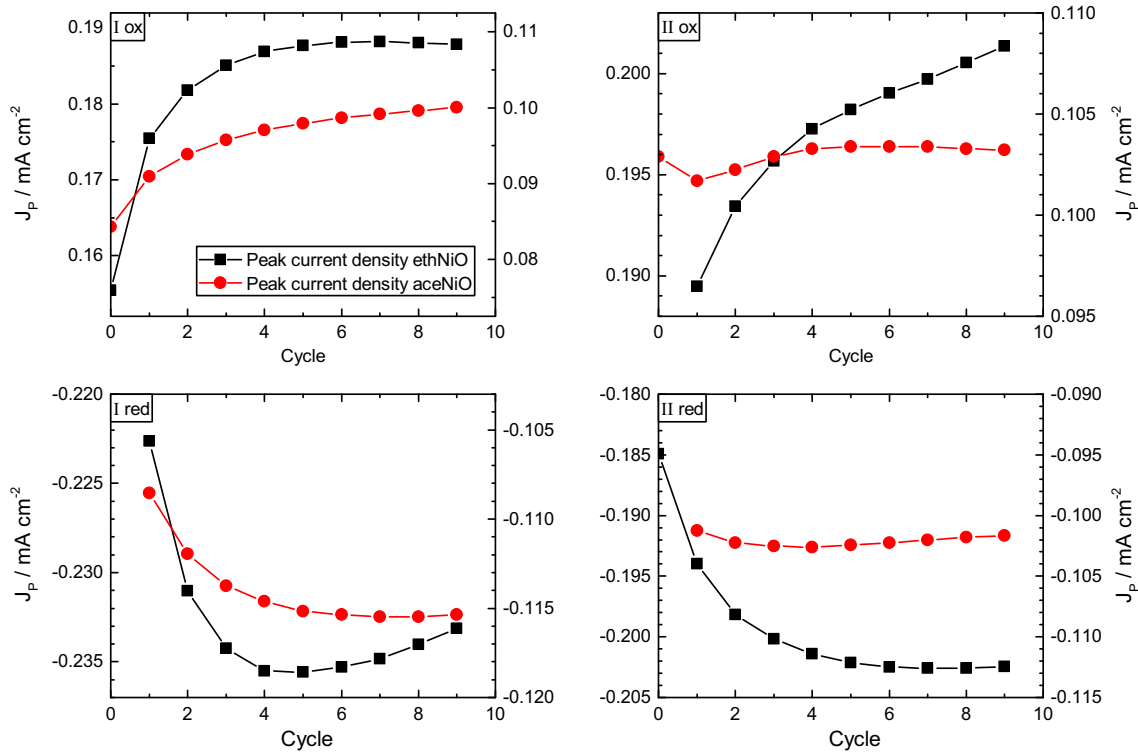


**Figure 6** Extracted peak current densities from the reduction and oxidation peaks for each cycle for ethNiO (black squares, left axes) and aceNiO (red circles, right axes) with identical step sizes but different current ranges for the axes of a given peak.

transparency and of 16.9 s to reach 90% of the maximum absorbance at 550 nm are in a typical range for NiO [50, 51, 56–58]. However, both materials suffer from chemical instability even within the first 5 cycles under the present conditions. This problem was stated also earlier, albeit at higher cycle numbers but less intense changes in transmission [48].

In order to discuss the efficiency of a material as an electrochromic layer, the observed change in transmission of a layer in contact to a given electrolyte should be compared to the charge exchanged. From Eq. (2) it directly follows that a high coloration efficiency is achieved for large changes in transmission at small charge uptake. The values of  $Q/V$  in Table 1 can be used to discuss the level of charging of the films at which this change in transmission was observed. Among the low-temperature, solution-based films, ethNiO provided most complete charging of the film ( $158 \text{ C cm}^{-3}$ ) at the given CE, slightly higher than aceNiO ( $63 \text{ C cm}^{-3}$ ) or NiO prepared from nanoparticles ( $89 \text{ C cm}^{-3}$ ) [50]. As another relevant criterion, significantly high charge uptake in a given film area  $Q/A$  is needed in order to qualify as an anode for, e.g.,  $\text{WO}_3$  as electrochromic cathode, for

which  $4 \text{ mC cm}^{-2}$  to  $50 \text{ mC cm}^{-2}$  are desirable [67–70]. NiO-layers characterised in  $\text{OH}^-$ -based electrolytes often show a higher charge density (see Table S1) but this electrolyte is incompatible to electrochromic switching of  $\text{WO}_3$  and, therefore, the present films are compared to those in Table 1.  $Q/A$  in Table 1 represents the charge uptake for which CE was determined and is of interest to discuss the methods regarding a good combination of high CE and high  $Q/A$ . NiO layers from the spray pyrolysis technique offer the highest  $Q/A$  in this comparison at, however, rather high temperatures during processing and moderate CE. Low-temperature NiO-layers with a high CE like the nanoparticle NiO show rather small  $Q/A$ . In comparison, the present ethNiO and aceNiO may offer a good compromise of a decent CE at moderate  $Q/A$ . An optimum has to be established because CE of NiO across methods of film preparation typically drops with increased  $Q/A$  or  $Q/V$ . This was also seen in chronoamperometric experiments (Fig. 8) with ethNiO- and aceNiO-layers, for which  $Q_{\text{max}}/A$  values of  $114 \text{ mC cm}^{-2}$  and  $46 \text{ mC cm}^{-2}$  were achieved at, however, decreased CE around  $4 \text{ cm}^2 \text{ C}^{-1}$  and  $10 \text{ cm}^2 \text{ C}^{-1}$ , respectively. The

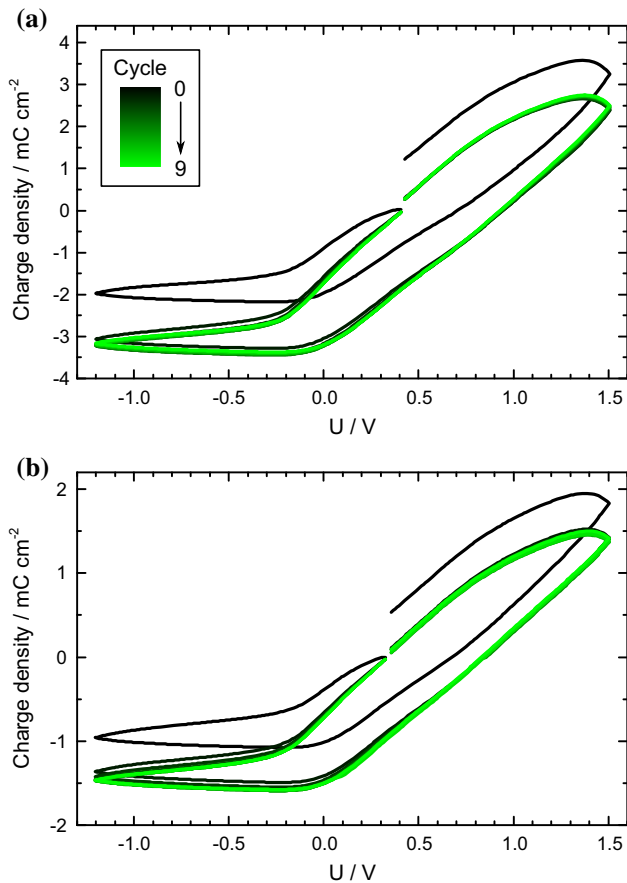


**Figure 7** Charge densities calculated from the measured current densities during cyclic voltammetry of ethNiO (a) and aceNiO (b) films.

corresponding maximum achieved volume charge densities ( $Q_{\max}/V$ ) of  $3260 \text{ C cm}^{-3}$  and  $1020 \text{ C cm}^{-3}$  compare favourably to values of  $180 \text{ C cm}^{-3}$  and  $690 \text{ C cm}^{-3}$  calculated from published values (Table 1). Optimum working conditions considering both parameters CE and  $Q/A$ , therefore, have to be established for each given type of device and application. The values of CE,  $Q/A$  and  $Q/V$  in Table 1 (and Table S1) can serve as benchmark values for choosing an appropriate preparation method for an envisaged device.

## Conclusions

We have demonstrated that the preparation of NiO layers by a combustion reaction of urea and nickel nitrate as fuel and oxidizer leads to very attractive film formation even at low processing temperatures. It is strongly influenced by the solvent used in the

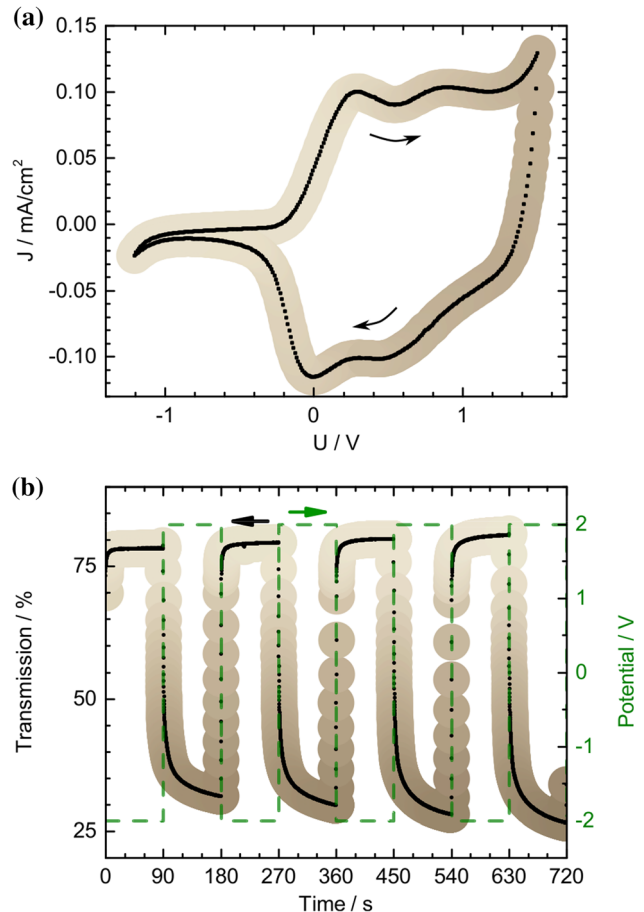


**Figure 8** Optical impression of aceNiO for a) the 9th cycle of a cyclic voltammogram and b) together with the transmission at 550 nm (black, left scale) at applied potential steps of  $-2 \text{ V}$  and  $2 \text{ V}$  each for 90 s (green, right scale). In both graphs the black points represents the data points, which are surrounded by the corresponding colours calculated from the collected spectra and calculated by the method described in the supplemental.

precursor solution. Such impact of the solvent indicates that the mechanism for the combustion reaction of nickel nitrate and urea as depicted in Eq. (1) is not complete for the presently presented reaction in dried layers but may show an additional input from solvent or film texture. Ethanol as solvent leads to more compact grainy films with a thickness of approximately 350 nm and a low general transparency. On the contrary, NiO layers prepared from acetone-based precursor solutions are porous and show a high transparency despite a thickness of approximately 450 nm. Both films have the necessary thickness to serve as a counter electrode for typical electrochromic tungsten oxide films and can be prepared below  $250 \text{ }^\circ\text{C}$ . The transmission could be

reversibly changed by about 25 and 34% at 550 nm for the ethNiO and aceNiO samples, respectively. This leads to a colouration efficiency of  $47.1 \text{ cm}^2 \text{ C}^{-1}$  for ethNiO and a remarkable high efficiency of  $92.3 \text{ cm}^2 \text{ C}^{-1}$  for aceNiO during cycling, which belong to the highest CE values reported in the literature for NiO in contact to  $\text{LiClO}_4/\text{PC}$  so far. These changes in colouration can be considered attractive for an addition of a counter anode to the  $55 \text{ cm}^2 \text{ C}^{-1}$  typically reached when switching  $\text{WO}_3$  cathodically. In addition, the blue characteristics of coloured  $\text{WO}_3$  devices might be spectrally broadened by the use of these NiO layers as counter electrodes to  $\text{WO}_3$ . The method presented here, therefore, shows the usefulness of solvents in a combustion reaction for NiO film preparation and their potential application in electrochromic devices. It may, therefore, help to reduce the production costs of electrochromic windows and glasses, broaden their commercial application and contribute to energy-saving solutions in architecture.

### Supplementary information

Extended information about the calculation of the colors for the graphical representation of the samples from the recorded spectra can be found in the supplementary information as well as a table with a comparison of the presently achieved characteristics (in analogy to Table 1) with reported data on different NiO films in contact to  $\text{OH}^-$  based electrolytes.

### Acknowledgements

Open Access funding provided by Projekt DEAL. The authors are grateful for financial support by the Federal State of Hesse (via “STORE-E” as part of the LOEWE program of excellence) as well as by Deutsche Forschungsgemeinschaft (via the project “SCHL340/19-1” and via the GRK 2204 “Substitute Materials for sustainable Energy Technologies”), for experimental support by the MiNa laboratory of LaMa/ZfM (Univ. Giessen) and for technical support by the machine-shop of the Physics Department (Univ. Giessen). We also thank Omeir Khalid (Inst. of Physical Chemistry, Univ. Giessen) for the TGA and DTA measurements.

### Compliance with ethical standards

**Conflict of interest** There are no conflict to declare.

**Electronic supplementary material:** The online version of this article (<https://doi.org/10.1007/s10853-020-04995-8>) contains supplementary material, which is available to authorized users.

**Open Access** This article is licensed under a Creative Commons Attribution 4.0 International License, which permits use, sharing, adaptation, distribution and reproduction in any medium or format, as long as you give appropriate credit to the original author(s) and the source, provide a link to the Creative Commons licence, and indicate if changes were made. The images or other third party material in this article are included in the article’s Creative Commons licence, unless indicated otherwise in a credit line to the material. If material is not included in the article’s Creative Commons licence and your intended use is not permitted by statutory regulation or exceeds the permitted use, you will need to obtain permission directly from the copyright holder. To view a copy of this licence, visit <http://creativecommons.org/licenses/by/4.0/>.

### References

- [1] Commission E (2011) Energy 2020: a strategy for competitive, sustainable, and secure energy. Publications Office, Luxembourg
- [2] Persson U, Werner S (2015) Stratego enhanced heating & cooling plans: quantifying the heating and cooling demand in Europe. Work Package 2, Background Report 4, Halmstad, Sweden
- [3] Commission E (2010) Directive 2010/31/EU of the European Parliament and of the Council of 19 May 2010 on the energy performance of buildings. OJEU 53(L 153):13–35
- [4] Kazanci OB, Olesen BW (2014) Sustainable plus-energy houses: final report
- [5] Jiang Y, Liu X, Zhang L, Zhang T (2015) High temperature cooling and low temperature heating in buildings of EBC annex 59. Energy Build 78:2433–2438
- [6] Kk G, Saboor S, Kumar V, Kim K-H, Babu TPA (2018) Experimental and theoretical studies of various solar control window glasses for the reduction of cooling and heating loads in buildings across different climatic regions. Energy Build 173:326–336

- [7] Aguilar-Santana JL, Jarimi H, Velasco-Carrasco M, Riffat S (2020) Review on window-glazing technologies and future prospects. *Int J Low-Carbon Tec* 15(1):112–120
- [8] Oh M, Tae S, Hwang S (2018) Analysis of heating and cooling loads of electrochromic glazing in high-rise residential buildings in South Korea. *Sustainability* 10(4):1121
- [9] Prüfbericht: MD-15/527/GL-K (2016) Kiwa GmbH, Magdeburg. [https://www.econtrol-glas.de/fileadmin/econtrol-glas/dateien/technische\\_dokumente/DB\\_15527-K\\_Econtrol\\_smart\\_3fach\\_ISO.PDF](https://www.econtrol-glas.de/fileadmin/econtrol-glas/dateien/technische_dokumente/DB_15527-K_Econtrol_smart_3fach_ISO.PDF). Accessed 16 Apr 2020
- [10] Lee ES, Selkowitz SE, Clear RD, DiBartolomeo DL, Klems JH, Fernandes LL, Ward GJ, Inkarojrit V, Yazdani M (2006) Advancement of electrochromic windows, Berkeley, CA
- [11] Applications for buildings around the globe (2020) Compagnie de Saint-Gobain. <https://www.sageglass.com/eu/applications>. Accessed 10 May 2020
- [12] EControl - Referenzen (2020) EControl-Glas GmbH & Co. KG. <https://www.econtrol-glas.de/referenzen/objektgalerie/>. Accessed 10 May 2020
- [13] Dimmable Glass (2020) Gentex Corporation. <https://www.gentex.com/products-technology/automotive/dimmable-glass/>. Accessed 10 May 2020
- [14] Barratt J, Dowd K (2006) A New Airplane for a New World: The Boeing 787 Dreamliner. *Design Management Review* 17(4):25–30
- [15] FADES® Sunglasses (2020) AshChromics. <https://ashchromics.com/products/fades-sunglasses?variant=31640172429391>. Accessed 20 May 2020
- [16] Niklasson GA, Granqvist CG (2007) Electrochromics for smart windows: thin films of tungsten oxide and nickel oxide, and devices based on these. *J Mater Chem* 17(2):127–156
- [17] Mortimer RJ (2011) Electrochromic Materials. *Annu Rev Mater Res* 41(1):241–268
- [18] Green S, Backholm J, Georén P, Granqvist CG, Niklasson GA (2009) Electrochromism in nickel oxide and tungsten oxide thin films: ion intercalation from different electrolytes. *Sol Energy Mater Sol Cells* 93(12):2050–2055
- [19] Sequeira CAC, Santos DMF (2010) Tungsten Oxide Electrochromic Windows with Lithium Polymer Electrolytes. *J Electrochem Soc* 157(6):J202–J207
- [20] Gillaspie DT, Tenent RC, Dillon AC (2010) Metal-oxide films for electrochromic applications: present technology and future directions. *J Mater Chem* 20(43):9585–9592
- [21] Granqvist CG (2014) Electrochromics for smart windows: oxide-based thin films and devices. *Thin Solid Films* 564:1–38
- [22] Zheng F, Kotobuki M, Song S, Lai MO, Lu L (2018) Review on solid electrolytes for all-solid-state lithium-ion batteries. *J Power Sources* 389:198–213
- [23] Sbar N, Badding M, Budziak R, Cortez K, Laby L, Michalski L, Ngo T, Schulz S, Urbanik K (1999) Progress toward durable, cost effective electrochromic window glazings. *Sol Energy Mater Sol Cells* 56(3–4):321–341
- [24] Dong D, Wang W, Rougier A, Barnabé A, Dong G, Zhang F, Diao X (2018) Lithium trapping as a degradation mechanism of the electrochromic properties of all-solid-state WO<sub>3</sub>/NiO devices. *J Mater Chem C* 6(37):9875–9889
- [25] Song X, Dong G, Gao F, Xiao Y, Liu Q, Diao X (2015) Properties of NiO<sub>x</sub> and its influence upon all-thin-film ITO/NiO<sub>x</sub>/LiTaO<sub>3</sub>/WO<sub>3</sub>/ITO electrochromic devices prepared by magnetron sputtering. *Vacuum* 111:48–54
- [26] Wang J-Y, Wang M-C, Jan D-J (2015) A Flexible Quasi-solid-state electrochromic device with polymeric electrolyte and WO<sub>3</sub>/NiO complementary system. *J Mater Sci Chem Eng* 03(07):136–141
- [27] Zhang J, Tu JP, Xia XH, Qiao Y, Lu Y (2009) An all-solid-state electrochromic device based on NiO/WO<sub>3</sub> complementary structure and solid hybrid polyelectrolyte. *Sol Energy Mater Sol Cells* 93(10):1840–1845
- [28] Lee SJ, Lee T-G, Nahm S, Kim DH, Yang DJ, Han SH (2020) Investigation of all-solid-state electrochromic devices with durability enhanced tungsten-doped nickel oxide as a counter electrode. *J Alloy Compd* 815:152399
- [29] Meng Z, Huang Y, Fang Y, Wang X, Guo Y, Liu Z, Xi M, Su W, Wang L (2019) Facile preparation of praseodymium oxide coated peanut-like lithium nickel cobalt manganese oxide microspheres for lithium ion batteries with high voltage capabilities. *J Alloy Compd* 784:620–627
- [30] Wei Z, Zhao T, Zhu X, An L, Tan P (2015) Integrated porous cathode made of pure perovskite lanthanum nickel oxide for nonaqueous lithium-oxygen batteries. *Energy Technol* 3(11):1093–1100
- [31] Patel KJ, Bhatt GG, Ray JR, Suryavanshi P, Panchal CJ (2017) All-inorganic solid-state electrochromic devices: a review. *J Solid State Electr* 21(2):337–347
- [32] Zhao B, Zhang X, Dong G, Wang H, Yan H (2015) Efficient electrochromic device based on sol–gel prepared WO<sub>3</sub> films. *Ionics* 21(10):2879–2887
- [33] Su Y, Zhang J, Shokhovets S, Polity A, Meyer BK (2017) Spectroscopic ellipsometry and optical transmission study of LiPON thin films prepared by RF sputtering. *Phys Status Solid B* 254(4):1600424
- [34] Su Y, Falgenhauer J, Polity A, Leichtweiß T, Kronenberger A, Obel J, Zhou S, Schlettwein D, Janek J, Meyer BK (2015) LiPON thin films with high nitrogen content for application

- in lithium batteries and electrochromic devices prepared by RF magnetron sputtering. *Solid State Ion* 282:63–69
- [35] Le Van-Jodin L, Ducroquet F, Sabary F, Chevalier I (2013) Dielectric properties, conductivity and Li<sup>+</sup> ion motion in LiPON thin films. *Solid State Ionics* 253:151–156
- [36] Ribeiro JF, Sousa R, Carmo JP, Gonçalves LM, Silva MF, Silva MM, Correia JH (2012) Enhanced solid-state electrolytes made of lithium phosphorous oxynitride films. *Thin Solid Films* 522:85–89
- [37] Browne MP (2016) Electrochromic nickel oxide films for smart window applications. *Int J Electrochem Sci* 11:6636–6647
- [38] Azaceta E, Tuyen NT, Pickup DF, Rogero C, Ortega JE, Miguel O, Grande H-J, Tena-Zaera R (2013) One-step wet chemical deposition of NiO from the electrochemical reduction of nitrates in ionic liquid based electrolytes. *Electrochim Acta* 96:261–267
- [39] Wu M-S, Huang Y-A, Jow J-J, Yang W-D, Hsieh C-Y, Tsai H-M (2008) Anodically potentiostatic deposition of flaky nickel oxide nanostructures and their electrochemical performances. *Int J Hydrogen Energ* 33(12):2921–2926
- [40] Chayasombat B, Yordsri V, Oikawa T, Thanachayanont C (2015) Microstructural characterization of nickel hydroxide films deposited using an ammonia-induced method and subsequently calcined nickel oxide films. *Mat Sci Semicon Proc* 34:224–229
- [41] Zhang X, Zhang Y, Zhao B, Lu S, Wang H, Liu J, Yan H (2015) Improvement on optical modulation and stability of the NiO based electrochromic devices by nanocrystalline modified nanocomb hybrid structure. *RSC Adv* 5(123):101487–101493
- [42] Huang H, Tian J, Zhang WK, Gan YP, Tao XY, Xia XH, Tu JP (2011) Electrochromic properties of porous NiO thin film as a counter electrode for NiO/WO<sub>3</sub> complementary electrochromic window. *Electrochim Acta* 56(11):4281–4286
- [43] Xia XH, Tu JP, Zhang J, Wang XL, Zhang WK, Huang H (2008) Electrochromic properties of porous NiO thin films prepared by a chemical bath deposition. *Sol Energy Mater Sol Cells* 92(6):628–633
- [44] Yates HM, Hodgkinson JL, Meroni SMP, Richards D, Watson TM (2020) Flame Assisted Chemical Vapour Deposition of NiO hole transport layers for planar perovskite cells. *Surf Coat Technol* 385:125423
- [45] Yates HM, Meroni SMP, Raptis D, Hodgkinson JL, Watson TM (2019) Flame assisted chemical vapour deposition NiO hole transport layers for mesoporous carbon perovskite cells. *J Mater Chem C* 7(42):13235–13242
- [46] Sialvi MZ, Mortimer RJ, Wilcox GD, Teridi AM, Varley TS, Wijayantha KG, Upul KCA (2013) Electrochromic and colorimetric properties of nickel(II) oxide thin films prepared by aerosol-assisted chemical vapor deposition. *ACS Appl Mater Interfaces* 5(12):5675–5682
- [47] Liu Q, Chen Q, Zhang Q, Xiao Y, Zhong X, Dong G, Delplancke-Ogletree M-P, Terryn H, Baert K, Reniers F, Diao X (2018) In situ electrochromic efficiency of a nickel oxide thin film: origin of electrochemical process and electrochromic degradation. *J Mater Chem C* 6(3):646–653
- [48] Wen R-T, Granqvist CG, Niklasson GA (2015) Anodic electrochromism for energy-efficient windows: cation/anion-based surface processes and effects of crystal facets in nickel oxide thin films. *Adv Funct Mater* 25(22):3359–3370
- [49] Wen R-T, Niklasson GA, Granqvist CG (2014) Electrochromic nickel oxide films and their compatibility with potassium hydroxide and lithium perchlorate in propylene carbonate: optical, electrochemical and stress-related properties. *Thin Solid Films* 565:128–135
- [50] Xie Z, Liu Q, Lu B, Zhai J, Diao X (2019) Large coloration efficiency and fast response NiO electrochromic thin film electrode based on NiO nanocrystals. *Mater Today Commun* 21:100635
- [51] Zhou J, Luo G, Wei Y, Zheng J, Xu C (2015) Enhanced electrochromic performances and cycle stability of NiO-based thin films via Li–Ti co-doping prepared by sol–gel method. *Electrochim Acta* 186:182–191
- [52] Cerc Korošec R, Felicijan M, Žener B, Pompe M, Dražić G, Padežnik Gomilšek J, Pihlar B, Bukovec P (2017) The role of thermal analysis in optimization of electrochromic effect of nickel oxide thin films, prepared by the sol-gel method: part III. *Thermochim Acta* 655:344–350
- [53] Liu A, Zhu H, Guo Z, Meng Y, Liu G, Fortunato E, Martins R, Shan F (2017) Solution Combustion Synthesis: low-temperature processing for p-Type Cu:NiO thin films for transparent electronics. *Adv Mater*. 29:1701599
- [54] Zhang Y, Li Z (2016) Low-temperature fabrication of sol–gel NiO film for optoelectronic devices based on the ‘fuel’ of urea. *Ceram Int* 42(5):6360–6368
- [55] Bai S, Cao M, Jin Y, Dai X, Liang X, Ye Z, Li M, Cheng J, Xiao X, Wu Z, Xia Z, Sun B, Wang E, Mo Y, Gao F, Zhang F (2014) Low-temperature combustion-synthesized nickel oxide thin films as hole-transport interlayers for solution-processed optoelectronic devices. *Adv Energy Mater*. 4:1301460
- [56] Tenent RC, Gillaspie DT, Miedaner A, Parilla PA, Curtis CJ, Dillon AC (2010) Fast-switching electrochromic Li<sup>+</sup>-doped NiO films by ultrasonic spray deposition. *J Electrochem Soc* 157(3):H318–H322
- [57] Ma D, Shi G, Wang H, Zhang Q, Li Y (2013) Hierarchical NiO microflake films with high coloration efficiency, cyclic stability and low power consumption for applications in a



- complementary electrochromic device. *Nanoscale* 5(11):4808–4815
- [58] Denayer J, Bister G, Simonis P, Colson P, Maho A, Aubry P, Vertruyen B, Henrist C, Lardot V, Cambier F, Cloots R (2014) Surfactant-assisted ultrasonic spray pyrolysis of nickel oxide and lithium-doped nickel oxide thin films, toward electrochromic applications. *Appl Surf Sci* 321:61–69
- [59] Chang J-Y, Chen Y-C, Wang C-M, Chen Y-W (2020) Electrochromic properties of Li-doped NiO films prepared by RF magnetron sputtering. *Coatings* 10(1):87
- [60] González-Cortés SL, Imbert FE (2013) Fundamentals, properties and applications of solid catalysts prepared by solution combustion synthesis (SCS). *Appl Catal A-Gen* 452:117–131
- [61] Varma A, Mukasyan AS, Rogachev AS, Manukyan KV (2016) Solution combustion synthesis of nanoscale materials. *Chem Rev* 116(23):14493–14586
- [62] Kim M-G, Hennek JW, Kim HS, Kanatzidis MG, Facchetti A, Marks TJ (2012) Delayed ignition of autocatalytic combustion precursors: low-temperature nanomaterial binder approach to electronically functional oxide films. *J Am Chem Soc* 134(28):11583–11593
- [63] Lide DR (ed) (2010) *CRC handbook of chemistry and physics on CD-ROM*, 2010th edn. CRC Press, Boca Raton
- [64] Mihelčič M, Šurca Vuk A, Jerman I, Orel B, Švegl F, Moulki H, Faure C, Campet G, Rougier A (2014) Comparison of electrochromic properties of  $\text{Ni}_{1-x}\text{O}$  in lithium and lithium-free aprotic electrolytes: from  $\text{Ni}_{1-x}\text{O}$  pigment coatings to flexible electrochromic devices. *Sol Energy Mat Sol C* 120:116–130
- [65] ECONTROL<sup>®</sup>—Switching behaviour of the dimmable glazing EControl-Glas GmbH & Co. KG. <https://www.econtrol-glas.de/en/knowledge-center/technology/switching-behaviour/>. Accessed 2 Apr 2020
- [66] SAGEGLASS<sup>®</sup> PRODUCT GUIDE: dynamic glass for a changing world (2016) SAGE Electrochromics I. [https://www.sageglass.com/sites/default/files/productguide\\_mkt\\_48.pdf](https://www.sageglass.com/sites/default/files/productguide_mkt_48.pdf). Accessed 13 Apr 2020
- [67] Wen-Cheun AuB, Chan K-Y, Knipp D (2019) Effect of film thickness on electrochromic performance of sol-gel deposited tungsten oxide ( $\text{WO}_3$ ). *Opt Mater* 94:387–392
- [68] Evecan D, Kaplan ŞS, Sönmez MŞ, Yıldırım S, Okutan M, Deligöz H, Zayim E (2019) Smart glass electrochromic device fabrication of uniform tungsten oxide films from its powder synthesized by solution combustion method. *Microelectron Eng* 215:110989
- [69] Pan J, Wang Y, Zheng R, Wang M, Wan Z, Jia C, Weng X, Xie J, Deng L (2019) Directly grown high-performance  $\text{WO}_3$  films by a novel one-step hydrothermal method with significantly improved stability for electrochromic applications. *J Mater Chem A* 7(23):13956–13967
- [70] Arvizu MA, Qu H-Y, Cindemir U, Qiu Z, Rojas-González EA, Primetzhofer D, Granqvist CG, Österlund L, Niklasson GA (2019) Electrochromic  $\text{WO}_3$  thin films attain unprecedented durability by potentiostatic pretreatment. *J Mater Chem A* 7(6):2908–2918

**Publisher's Note** Springer Nature remains neutral with regard to jurisdictional claims in published maps and institutional affiliations.